Competition of spatially inhomogeneous phases in systems with nesting-driven spin-density wave state

S. V. Kokanova,[1] P. A. Maksimov,[2] A. V. Rozhkov,[3] and A. O. Sboychakov[3]
[1]*Skolkovo Institute of Science and Technology, Moscow 143026, Russia*
[2]*Bogolyubov Laboratory of Theoretical Physics, Joint Institute for Nuclear Research, Dubna, Moscow Region 141980, Russia*
[3]*Institute for Theoretical and Applied Electrodynamics, Russian Academy of Sciences, Moscow 125412, Russia*

(Received 9 November 2020; revised 13 July 2021; accepted 13 July 2021; published 6 August 2021)

At low temperature, a fermionic system with perfectly nested Fermi surface orders into a spin-density wave. Upon doping, however, the latter state becomes unstable, and several spatially inhomogeneous phases emerge competing against each other to become the true ground state. We investigate this competition using the anisotropic Hubbard model on a three-dimensional cubic lattice in a weak-coupling regime as a convenient study case. For this model it is known that, at half-filling (one electron per site), the Fermi surface nesting is perfect, and the ground state is the commensurate spin-density wave. Away from the half-filling, various types of spatially inhomogeneous phases, such as phase-separated states and the state with domain walls ("soliton lattice"), emerge. Using the mean-field theory, we evaluate the free energies of these phases to determine which of them could become the true ground state. Our study demonstrates that the free energies of all discussed states are very close to each other. Smallness of these energy differences suggests that, for a real material, numerous factors, unaccounted by the model, may arbitrary shift the relative stability of the competing phases. We further argue that purely theoretical prediction of a structure of inhomogeneous phase in a particular doped system is unreliable.

DOI: 10.1103/PhysRevB.104.075110

I. INTRODUCTION

Investigations of inhomogeneous electronic states of different types constitute an active research area of modern condensed matter physics [1–23]. In this work, we specifically focus our attention on inhomogeneous states hosted by doped antiferromagnetic (AFM) or spin-density wave (SDW) insulator. In the most general sense, this physical situation is of interest for cuprates [24–28], manganites [29–33], pnictides [12,34–36], the Bechgaard salts [18–23], among others. (Related phenomenon may be observed in some nonmagnetic superconducting systems [17] as well.) For doped AFM/SDW materials, inhomogeneities of several types (e.g., domain walls, or "stripes", spatial separation into several nonidentical phases, "checkerboard" state, as well as others) are discussed [10,18,21–24,34,37–42].

Many-body states hosting these types of inhomogeneities commonly occur in theoretical and numerical research [14–16,38,43–49]. Often, various inhomogeneous phases compete against each other to become the true ground state of a model Hamiltonian. The outcome of this competition is usually presented [15,16,38,43] as a phase diagram that depicts how various states, both homogeneous and inhomogeneous, replace each other upon parameters variations. Yet, when comparing the model phase diagram against experimental data, one inevitably has to address the following question: to which extent the diagram calculated within a simplified theoretical framework with the help of inexact tools is robust in the presence of various perturbations unaccounted by the model, or distortions and artifacts introduced by the approximations?

Answering this question, it is often implicitly assumed that, although some variability of the phase boundaries is indeed unavoidable, the qualitative features of the diagram survive the reality check. In the context of the cuprates and the manganites, however, it was argued [50] that the situation might not be that straightforward: The presence of several competing states with close energies make it possible for a weak perturbation, such as disorder or external pressure, to induce drastic changes in the ground-state structure. Several papers [46–48] including recent state-of-the-art numerical studies [44,45,49] reiterated this concern. For example, Ref. [45] emphasized the smallness of energy difference separating contending phases, remarking that discrepancies between numerical results and experimental data could be a consequence of certain contributions neglected by the model Hamiltonian.

Unfortunately, for cuprates, a detailed analysis of this competition is painfully difficult. The root of the problem here is strong electron-electron interaction, a distinctive aspect of cuprates and similar materials. Strong interaction forces one to rely on uncontrollable approximations, or highly specialized custom-made numerical tools. Yet adequate description of the inhomogeneous phases competition remains relevant theoretical issue beyond the realm of systems with strong coupling. Various materials believed to be in a weak-coupling regime (most notably, iron-based pnictide superconductors and Bechgaard salts), host inhomogeneous states emerging against the backdrop of a parent SDW. As we will see below,

the study of the inhomogeneous states competition at weak electron-electron interaction is a much more tractable task amenable to general physics methods.

One must remember that, to stabilize the SDW phase in a weak-coupling model, Fermi surface nesting is necessary. At perfect (or near-perfect) nesting, the SDW order is robust, and can be consistently described [15,35,36,51–71] within the mean-field approximation. Upon doping the SDW state becomes unstable with respect to formation of inhomogeneous phases. The following phases are typically discussed in the literature: (i) real-space separation into the paramagnetic state and commensurate SDW; (ii) separation into commensurate and incommensurate SDW phases; and (iii) a phase with domain walls (sometimes called "soliton lattice" or "soliton phase"), see, for example, Refs. [15,35–37,43,62,64,72,73]. The energies of (i)–(iii) can be readily evaluated, and the competition can be minutely scrutinized, much unlike the regime of strong coupling.

Below we focus our attention on the inhomogeneous phase competition for an SDW system with weak interaction. The outline of the investigation is as follows. We adopt the Hubbard model with small interaction parameter U/t as a study case (a continuous-space Hamiltonian [36,51] could be also used, yet, natural discretization of a lattice model is an advantage for numerical calculations). We investigate the relative stability of the inhomogeneous states (i)–(iii). To determine which of them is energetically favorable, it is necessary to compare the states' free energies F, the latter being calculated using the mean-field approximation. It is found that for all three states the values of F are virtually identical, at least at small doping. This finding and its implications are the main focus of this paper.

Our presentation is organized as follows. General mean-field approximation specialized for the Hubbard model at finite doping is introduced in Sec. II. In Sec. III we present calculations for the phase-separated states. The application of the mean-field approximation to the state with domain walls is explained in Sec. IV. Section V is dedicated to the discussion of the results. Some auxiliary results are relegated to two Appendices.

II. MEAN-FIELD APPROACH FOR THE HUBBARD MODEL

We consider antiferromagnetic state of anisotropic Hubbard model on a three-dimensional (3D) cubic lattice in the weak-coupling regime. The Hamiltonian of the model equals to

$$H = \sum_{\langle ij\rangle\sigma} t_{ij}(c^\dagger_{i\sigma}c_{j\sigma} + \text{H.c.}) - \mu\sum_{i\sigma} c^\dagger_{i\sigma}c_{i\sigma} + \\ + U\sum_i \left(n_{i\uparrow} - \frac{1}{2}\right)\left(n_{i\downarrow} - \frac{1}{2}\right), \tag{1}$$

where $c^\dagger_{i\sigma}$ and $c_{i\sigma}$ are the creation and annihilation operators for an electron with spin projection $\sigma =\uparrow, \downarrow$ located in the site i, local density operator is $n_{i\sigma} = c^\dagger_{i\sigma}c_{i\sigma}$, notation $\langle ij\rangle$ implies that sites i and j are nearest neighbors, and t_{ij} represents the hopping amplitude connecting sites i and j. To model anisotropy typical for the pnictides, the Bechgaard salts, as well as other materials, we assume that t_{ij} are different for different orientations of the $\langle ij\rangle$ bond: when the bond is parallel to the α axis ($\alpha = x, y, z$), the amplitude is $t_{ij} = t_\alpha$.

In the second term of Eq. (1), μ is the chemical potential. The last term in Eq. (1) describes on-site Coulomb repulsion of electrons with opposite spin projections, with the interaction constant $U > 0$. The terms $1/2$ in parentheses are added in order to chemical potential μ would equal to zero at half-filling (one electron per site).

We consider the Hubbard model (1) near the half-filling. At half-filling, the ground state of the Hubbard model is known to be antiferromagnetic [74]. It is assumed that small doping modifies but does not destroy the antiferromagnetic ordering.

Antiferromagnetic state is characterized by finite position-dependent order parameter

$$\Delta_i = \frac{U}{2}(\langle n_{i\uparrow}\rangle - \langle n_{i\downarrow}\rangle), \tag{2}$$

where $\langle\ldots\rangle$ denotes the ground-state matrix element. For the states with domain walls, the sum $\langle n_{i\uparrow}\rangle + \langle n_{i\downarrow}\rangle$ is also position-dependent. Thus, it is useful to introduce the local doping level

$$x_i = \langle n_{i\uparrow}\rangle + \langle n_{i\downarrow}\rangle - 1. \tag{3}$$

We study antiferromagnetic states of the model (1) in the weak-coupling regime, when $U < W$, where W is the bandwidth, $W = 4\sum_\alpha t_\alpha$. In this case, the mean-field approach is the appropriate method to study the model (1), as discussed in Appendix A. The mean field form of Hamiltonian (1) is

$$H = H_{\text{kin}} + H^{\text{MF}}_{\text{int}}, \tag{4}$$

$$H_{\text{kin}} = \sum_{\langle ij\rangle\sigma} t_{ij}(c^\dagger_{i\sigma}c_{j\sigma} + \text{H.c.}) - \sum_{i\sigma}\mu'_i c^\dagger_{i\sigma}c_{i\sigma}, \tag{5}$$

$$H^{\text{MF}}_{\text{int}} = \sum_i \left[\Delta_i(c^\dagger_{i\downarrow}c_{i\downarrow} - c^\dagger_{i\uparrow}c_{i\uparrow}) - U\left(\frac{x_i(2+x_i)}{4} - \frac{\Delta_i^2}{U^2}\right)\right], \tag{6}$$

where $\mu'_i = \mu - Ux_i/2$ is the effective (position-dependent) chemical potential, which accounts for both μ and "Hartree" contribution $Ux_i/2$. Parameters x_i and Δ_i are to be found self-consistently.

III. PHASE SEPARATED STATES

At zero doping the system's ground state is the homogeneous commensurate SDW. When electrons or holes are added, the homogeneous state may become unstable. In this section we will investigate two specific scenarios of this instability. For both scenarios we start assuming the stability of the doped homogeneous phase, and then invalidate this assumption.

A. Commensurate antiferromagnetism

In this subsection the phase separation into the commensurate SDW and the paramagnetic states is discussed. We assume that the doped system remains homogeneous $x_i = x =$ const., and the order parameter is commensurate:

$$\Delta_i = (-1)^{i_x+i_y+i_z}\Delta, \tag{7}$$

where $\Delta = \text{const.}$, and integers i_x, i_y, and i_z describe the position of the lattice site $i = (i_x, i_y, i_z)$. For Δ_i given by Eq. (7) we derive

$$H = \sum_{\mathbf{k}\sigma} (\varepsilon_{\mathbf{k}} - \mu') c^{\dagger}_{\mathbf{k}\sigma} c_{\mathbf{k}\sigma} + \\ + \sum_{\mathbf{k}} \Delta \left(c^{\dagger}_{\mathbf{k}\uparrow} c_{\mathbf{k}+\mathbf{Q}_0\uparrow} - c^{\dagger}_{\mathbf{k}\downarrow} c_{\mathbf{k}+\mathbf{Q}_0\downarrow} \right) - \\ - U\mathcal{N}\left(\frac{x(2+x)}{4} - \frac{\Delta^2}{U^2} \right), \tag{8}$$

where $\mu' = \mu - Ux/2$, the number of sites in the lattice is denoted by $\mathcal{N}$, vector $\mathbf{k} = (k_x, k_y, k_z)$ is the quasi-momentum, and

$$\varepsilon_{\mathbf{k}} = 2[t_x \cos(k_x) + t_y \cos(k_y) + t_z \cos(k_z)] \tag{9}$$

is the kinetic energy. At half-filling ($x = 0$, $\mu = \mu' \equiv 0$) the model's Fermi surface nests perfectly, with $\mathbf{Q}_0 = (\pi, \pi, \pi)$ as the nesting vector. Indeed, at the half-filling the Fermi surface is defined by the equation

$$\varepsilon_{\mathbf{k}} = 0, \tag{10}$$

which remains invariant under translation by $\mathbf{Q}_0$, as guaranteed by the relation

$$\varepsilon_{\mathbf{k}+\mathbf{Q}_0} = -\varepsilon_{\mathbf{k}}. \tag{11}$$

Note that this equation is valid for $\mu = 0$ only. Thus, finite doping destroys the perfect nesting. (Curiously, however, the nesting is insensitive to hopping anisotropy.)

The eigenenergies of Hamiltonian (8) can be easily found

$$E^{(1,2)}_{\mathbf{k}} = -\mu' \mp \sqrt{\varepsilon^2_{\mathbf{k}} + \Delta^2}. \tag{12}$$

At zero temperature, the grand potential per site is

$$\Omega = \sum_s \int \frac{d^3\mathbf{k}}{(2\pi)^3} E^{(s)}_{\mathbf{k}} \Theta\left(-E^{(s)}_{\mathbf{k}}\right) - U\left(\frac{x(2+x)}{4} - \frac{\Delta^2}{U^2} \right). \tag{13}$$

Minimizing Ω with respect to Δ the following equation relating Δ and μ' can be derived (details are presented in Appendix B)

$$|\mu'| + \sqrt{\mu'^2 - \Delta^2} = \Delta_0, \tag{14}$$

where

$$\Delta_0 = W \exp\left[-\frac{1}{\rho_0} \left(\frac{1}{U} - \frac{1}{U_c} \right) \right] \tag{15}$$

is the gap at half-filling (here, ρ_0 is the density of states at the Fermi level, and U_c is defined in Appendix B). Since a typical experiment is performed at fixed doping, not fixed chemical potential, it is necessary to express the order parameter and the chemical potential as functions of the doping level x. The doping x is given by the following relation:

$$x = \sum_s \int \frac{d^3\mathbf{k}}{(2\pi)^3} \Theta\left(-E^{(s)}_{\mathbf{k}}\right) - 1. \tag{16}$$

Acting in the same manner as described in Appendix B, we obtain in the weak-coupling limit

$$x = 2\rho_0 \text{sign}(\mu') \sqrt{\mu'^2 - \Delta^2}. \tag{17}$$

If we set $\Delta = 0$ in Eq. (17), we recover a familiar expression

$$\mu = \frac{x}{2\rho_0}, \tag{18}$$

which relates doping and chemical potential in the paramagnetic phase. In Eq. (18) the contribution $Ux/2$ to the effective potential is omitted. The effects due to this term are small in the weak-coupling limit, as we will show below.

Using Eqs. (14) and (17), and neglecting $Ux/2$ contribution to μ', we further obtain [37,51]

$$|\mu| = \Delta_0 \left(1 - \frac{|x|}{2\rho_0\Delta_0} \right), \tag{19}$$

$$\Delta = \Delta_0 \sqrt{1 - \frac{|x|}{\rho_0\Delta_0}}. \tag{20}$$

These two formulas describe homogeneous SDW state. We note that the chemical potential is the decreasing function of the doping

$$\frac{\partial\mu}{\partial x} = -\frac{1}{2\rho_0} < 0. \tag{21}$$

It means that the compressibility is negative and homogeneous SDW state is unstable, disproving the initial assumption of stability. This is the first example of the phase separation. Observe that the small correction to $\partial\mu/\partial x$ due to the omitted $Ux/2$ contribution to μ' cannot restore the stability of the homogeneous state as long as we consider the weak-coupling limit.

The structure of inhomogeneous phase can be established with the help of Maxwell construction, see Fig. 1. It shows the chemical potential of the homogeneous commensurate SDW state [decreasing line, Eq. (19)] and paramagnetic state [increasing line, Eq. (18)] versus the doping level. The horizontal line in Fig. 1 should be drawn so that areas S_1 and S_2 are equal. This line represents the phase-separated state. In thermodynamic equilibrium (that is, neglecting metastable states), the chemical potential of the this state is

$$\mu_{\text{cAF}} = \frac{\Delta_0}{\sqrt{2}} \approx 0.707\Delta_0, \tag{22}$$

where the subscript "cAF" stands for "commensurate antiferromagnet". The neglected $Ux/2$ term introduces small correction (of the order of $U\rho_0\Delta_0$) to the value of μ_{cAF}.

The physical meaning of μ_{cAF} is the threshold value which must be exceeded by the chemical potential of an external reservoir for doping to commence. The electrons injected into the SDW parent state, however, do not spread over the whole lattice evenly. Instead, as the Maxwell construction implies, the inhomogeneous state is split into areas of the undoped SDW and paramagnetic areas (the latter accumulate all the doping).

The main goal of this study is to determine which of the inhomogeneous states is energetically favorable. At fixed doping, this can be decided by comparison of the free energies $F(x) = \Omega + \mu x$ of the competing phases. For evaluation of $F(x)$, the following expression is useful

$$F(x) = F(0) + \int_0^x \mu(x')dx', \tag{23}$$

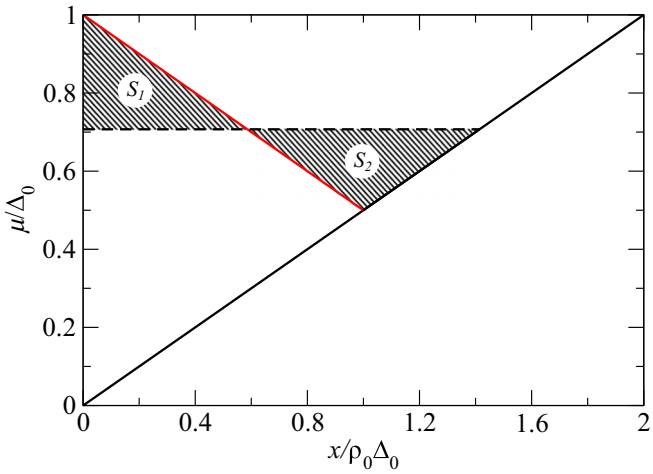

FIG. 1. The doping dependence of the chemical potential for the commensurate SDW and paramagnetic phases. Chemical potential μ and doping x are normalized by Δ_0 and $\rho_0\Delta_0$, correspondingly. From $x = 0$ to $x = \rho_0\Delta_0/2$ the chemical potential in the commensurate SDW phase is shown as a straight (red) line, see Eq. (19). Since this line has negative derivative, the doped commensurate SDW state is unstable. For the paramagnetic phase, $\mu = \mu(x)$ is shown as a straight (black) line, see Eq. (18). To determine the chemical potential of the phase-separated state, we use Maxwell construction: The horizontal dashed line is drawn to guarantee the equality of the areas $S_1 = S_2$. The chemical potential of the inhomogeneous state is $\Delta_0/\sqrt{2}$. As one can see from the Maxwell construction, the separation occurs into the undoped SDW and the paramagnetic phases.

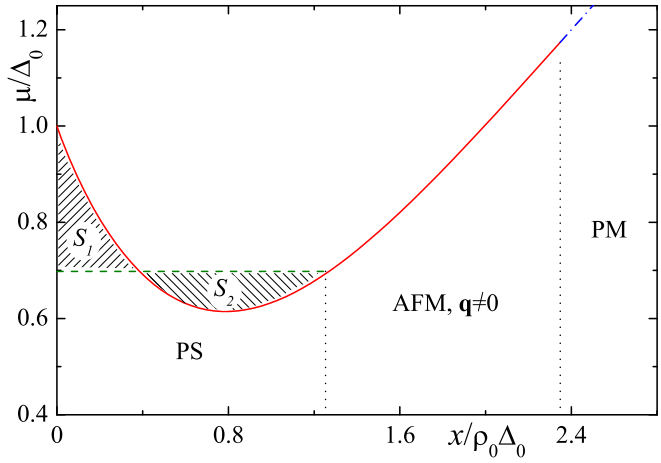

FIG. 2. The doping dependence of the chemical potential of the incommensurate SDW state (solid red curve) and the paramagnetic state (blue dot-dashed curve). The Maxwell's construction requires that the hatched areas $S_{1,2}$ are equal to each other. Horizontal dashed (green) line corresponds to the chemical potential of the phase-separated state. It equals to $\mu_{\rm iAF}/\Delta_0 \cong 0.698$. Model parameters are $t_x = t_y = 1$, $t_z = 0.7$, incommensurability vector $\mathbf{q}$ is parallel to the z axis.

where $F(0)$ is the free energy of undoped SDW insulator. Since the chemical potential is doping-independent in the phase-separated state, we derive

$$F_{\rm cAF}(x) = F(0) + \mu_{\rm cAF} x. \tag{24}$$

This expression is valid for sufficiently low doping, as long as the system remains on the horizontal line in Fig. 1. In the following sections, $F_{\rm cAF}$ will be compared with the free energies of other inhomogeneous states.

Finally, let us note that the long-range Coulomb interaction may arrest or drastically modify the phase separation into the regions of unequal electron density. This issue will be discussed in more details in Sec. V.

B. Incommensurate antiferromagnetism

We have seen in the previous section that at half-filling perfect nesting is realized at $\mathbf{Q}_0$. For finite doping the perfect nesting is impossible, but the quality of nesting may be improved if we consider incommensurate SDW, whose nesting vector is

$$\mathbf{Q} = \mathbf{Q}_0 + \mathbf{q} \tag{25}$$

where $\mathbf{q}$ is incommensurability vector. When $|\mathbf{q}|$ is finite, the order parameter takes the form

$$\Delta_i = U\langle c^\dagger_{i\uparrow} c_{i\downarrow}\rangle = \Delta(-1)^{i_x+i_y+i_z} e^{i\mathbf{q}\mathbf{r}_i}, \tag{26}$$

where $\mathbf{r}_i = (i_x,\ i_y,\ i_z)$. The interaction part of the mean-field Hamiltonian in k space becomes

$$H^{\rm MF}_{\rm int} = \sum_{\mathbf{k}} \Delta\left(c^\dagger_{\mathbf{k}\uparrow} c_{\mathbf{k}+\mathbf{Q}\downarrow} + c^\dagger_{\mathbf{k}+\mathbf{Q}\downarrow} c_{\mathbf{k}\uparrow}\right) - \\ - UN\left(\frac{x(2+x)}{4} - \frac{\Delta^2}{U^2}\right), \tag{27}$$

Taking into account the relation $\varepsilon_{\mathbf{k}+\mathbf{Q}} = -\varepsilon_{\mathbf{k}+\mathbf{q}}$, we can write the equations for eigenenergies

$$E^{(1,2)}_{\mathbf{k}} = -\mu' + \frac{\varepsilon_{\mathbf{k}} - \varepsilon_{\mathbf{k}+\mathbf{q}}}{2} \mp \sqrt{\left(\frac{\varepsilon_{\mathbf{k}} + \varepsilon_{\mathbf{k}+\mathbf{q}}}{2}\right)^2 + \Delta^2}. \tag{28}$$

Grand potential of the system per one site is given by Eq. (13) with eigenenergies from Eq. (28). The equations for the order parameter Δ, nesting vector $\mathbf{q}$, and the chemical potential are

$$\frac{\partial\Omega}{\partial\Delta} = 0, \quad \frac{\partial\Omega}{\partial\mathbf{q}} = 0, \quad -\frac{\partial\Omega}{\partial\mu'} = 1 + x. \tag{29}$$

These equations are solved [15,35,51] in the limit of small $|\mathbf{q}|$, see Appendix C for details.

The resultant dependence $\mu = \mu(x)$ calculated for $\mathbf{q}$ parallel to the z axis is plotted in Fig. 2. Here, as in the previous section, the small correction $Ux/2$ was neglected. We see nonmonotonic behavior of $\mu(x)$, indicating the instability of the homogeneous state toward the phase separation, analogous to what Fig. 1 has shown. This time, however, the separated phases are (undoped) commensurate and incommensurate SDW states, as one can prove using the Maxwell construction. The chemical potential of the inhomogeneous state is

$$\mu_{\rm iAF} \approx 0.698\Delta_0, \tag{30}$$

where the subscript "iAF" stands for "incommensurate antiferromagnet". When $\mathbf{q}$ is parallel to the y axis, the dependence

$\mu = \mu(x)$ is very similar to that shown in Fig. 2, except that the transition to the paramagnetic state in this case occurs at smaller doping.

Similar to $F_{\rm cAF}$, Eq. (24), the free energy $F_{\rm iAF}$ for the inhomogeneous phase represented by the horizontal line in Fig. 2 is

$$F_{\rm iAF}(x) = F(0) + \mu_{\rm iAF} x. \tag{31}$$

It is easy to see that

$$F_{\rm iAF}(x) < F_{\rm cAF}(x) \quad \Leftrightarrow \quad \mu_{\rm iAF} < \mu_{\rm cAF}. \tag{32}$$

Thus, the phase separation into the commensurate and incommensurate SDW phases is more favorable than the separation into the commensurate SDW state and the paramagnetic state.

It is interesting to note that Eq. (32) reduces the comparison of the free energies to the comparison of the critical chemical potentials $\mu_{\rm cAF}$ and $\mu_{\rm iAF}$. Since these quantities are very close to each other ($\mu_{\rm iAF} \cong 0.698\Delta_0$ vs $\mu_{\rm cAF} \cong 0.707\Delta_0$), the energy difference between these two inhomogeneous states is very small for all relevant values of x.

IV. A STATE WITH DOMAIN WALLS

A. General considerations

Yet another type of inhomogeneous phase competing to become the true ground state is the phase with domain walls. In the previous section we have seen that, to decide which phase-separated state is more energetically favorable, the critical chemical potentials have to be compared. In this section, we will calculate $\mu_{\rm dw}$, the critical chemical potential for the phase with domain walls.

When the system's chemical potential is close to the threshold value, the doping concentration is low (this is a direct consequence of the critical chemical potential definition). A phase with domain walls in such a regime is characterized by large interwall separation and negligible interaction between the domain walls. Thus, $\mu_{\rm dw}$ is determined by the properties of a single domain wall.

Beginning our study of an isolated domain wall, several considerations must be taken into account. An important characteristics of a domain wall is its orientation relative to lattice axes. The vector normal to the domain wall plane may be parallel to one of the crystallographic axes, or it may point in an arbitrary direction [75]. All these orientations cannot be investigated in complete generality, and the study scope must be restricted. Numerical calculations for the arbitrary orientations of the domain walls are computationally costly. We expect that, in agreement with previous publications [45] the domain walls whose normal vectors are parallel to one of the axis are the most stable.

We study two types of domain walls: bond-centered and site-centered. They can be schematically depicted with the help of the following one-dimensional cartoons

$$\uparrow\downarrow\uparrow\ \downarrow\downarrow\ \uparrow\downarrow\uparrow \quad \text{bond-centered domain wall,}$$
$$\uparrow\downarrow\uparrow\ \downarrow\ \text{o}\ \uparrow\ \downarrow\uparrow \quad \text{site-centered domain wall.}$$

The arrows here represent the direction of the on-site spin magnetization, the symbol "o" corresponds to a site with vanishing magnetization. Despite obvious differences in real-space structures, our numerical simulations show that the energies of bond-centered and site-centered configurations are very close to each other.

B. Mean-field description of a domain wall

Let us now outline the mean-field formalism we employ to study a single domain wall. For definiteness, we assume the domain wall is perpendicular to the x axis. For such an orientation, the translation invariance in y and z directions is preserved, while it is explicitly broken in x direction: the density of electrons and the order parameter are

$$\begin{aligned} &\langle n_{i\uparrow}\rangle + \langle n_{i\downarrow}\rangle = n_{i_x}, \\ &\Delta_i = \Delta_{i_x}(-1)^{i_y+i_z}. \end{aligned} \tag{33}$$

Therefore, it is convenient to switch to the mixed representation of $c^\dagger_{i\sigma}$ as follows

$$c^\dagger_{i_x\mathbf{p}\sigma} = \frac{1}{\sqrt{\mathcal{N}_y\mathcal{N}_z}} \sum_{i_y,i_z} c^\dagger_{i\sigma} e^{i(p_y i_y + p_z i_z)}. \tag{34}$$

Here $\mathbf{p} = (p_y,\ p_z)$ is the 2D quasi-momentum, $\mathcal{N}_\alpha$ is the number of unit cells along axis $\alpha = x, y, z$.

The mean-field Hamiltonian in the mixed representation reads

$$H = H_{\rm kin} + H^{\rm MF}_{\rm int}, \tag{35}$$

$$\begin{aligned} H_{\rm kin} = &\sum_{i_x\mathbf{p}\sigma} t_x\left(c^\dagger_{i_x\mathbf{p}\sigma} c_{i_x+1\mathbf{p}\sigma} + \text{H.c.}\right) + \\ &+ \sum_{i_x\mathbf{p}\sigma} \left(\varepsilon^\perp_{\mathbf{p}} - \mu'_{i_x}\right) c^\dagger_{i_x\mathbf{p}\sigma} c_{i_x\mathbf{p}\sigma}, \end{aligned} \tag{36}$$

$$\begin{aligned} H^{\rm MF}_{\rm int} = &-\sum_{i_x\mathbf{p}} \Delta_{i_x}\left(c^\dagger_{i_x\mathbf{p}\uparrow} c_{i_x\mathbf{p}+\mathbf{P}_0\uparrow} - c^\dagger_{i_x\mathbf{p}\downarrow} c_{i_x\mathbf{p}+\mathbf{P}_0\downarrow}\right) \\ &- U\frac{\mathcal{N}}{\mathcal{N}_x}\sum_{i_x}\left(\frac{n^2_{i_x}-1}{4} - \frac{\Delta^2_{i_x}}{U^2}\right), \end{aligned} \tag{37}$$

where $\mu'_{i_x} = \mu - U(n_{i_x} - 1)/2$. We also use the notations $\varepsilon^\perp_{\mathbf{p}} = -2t_y\cos(p_y) - 2t_z\cos(p_z)$ and $\mathbf{P}_0 = (\pi,\ \pi)$.

If we introduce the $2\mathcal{N}_x$-component vectors

$$\psi^\dagger_{\mathbf{p}\sigma} = \left(c^\dagger_{1\mathbf{p}\sigma}, \ldots,\ c^\dagger_{\mathcal{N}_x\mathbf{p}\sigma}, c^\dagger_{1\mathbf{p}+\mathbf{P}_0\sigma}, \ldots,\ c^\dagger_{\mathcal{N}_x\mathbf{p}+\mathbf{P}_0\sigma}\right), \tag{38}$$

the Hamiltonian (35) can be expressed as $H = \sum_{\mathbf{p}\sigma} \psi^\dagger_{\mathbf{p}\sigma} \hat{H}_{\mathbf{p}\sigma} \psi_{\mathbf{p}\sigma}$, where the matrices $\hat{H}_{\mathbf{p}\sigma}$ can be written in the following block form

$$\hat{H}_{\mathbf{p}\uparrow} = \begin{pmatrix} \hat{H}_{0\mathbf{p}} & \hat{\Delta} \\ \hat{\Delta} & \hat{H}_{0\mathbf{p}+\mathbf{P}_0} \end{pmatrix},\ \hat{H}_{\mathbf{p}\downarrow} = \begin{pmatrix} \hat{H}_{0\mathbf{p}} & -\hat{\Delta} \\ -\hat{\Delta} & \hat{H}_{0\mathbf{p}+\mathbf{P}_0} \end{pmatrix}. \tag{39}$$

In the latter formulas, the matrices $\hat{H}_{0\mathbf{p}}$ and $\hat{\Delta}$ are

$$\hat{H}_{0\mathbf{p}} = \begin{pmatrix} \varepsilon^\perp_{\mathbf{p}} - \mu'_1 & t & 0 & \cdots & t \\ t & \varepsilon^\perp_{\mathbf{p}} - \mu'_2 & t & \cdots & 0 \\ 0 & t & \varepsilon^\perp_{\mathbf{p}} - \mu'_3 & \cdots & 0 \\ \vdots & \vdots & \vdots & \ddots & \vdots \\ t & 0 & 0 & \cdots & \varepsilon^\perp_{\mathbf{p}} - \mu'_{\mathcal{N}_x} \end{pmatrix}, \tag{40}$$

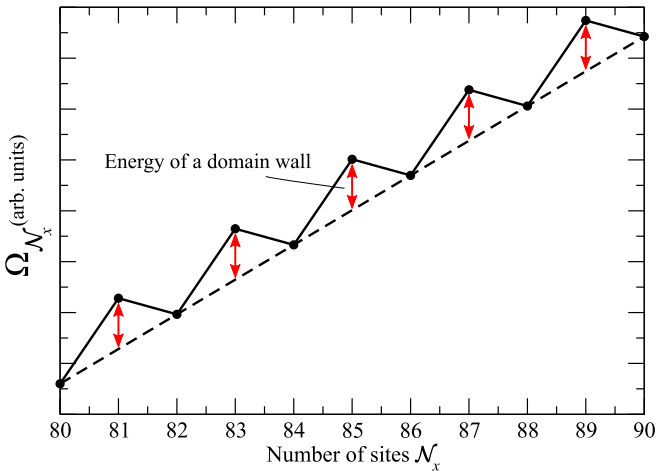

FIG. 3. Schematic illustration of the dependence of the grand potential $\Omega_{\mathcal{N}_x}$ on the number of sites in the x direction. For even $\mathcal{N}_x$, the dashed line represents proportionality $\Omega^{\rm even}_{\mathcal{N}_x} \propto \mathcal{N}_x$, see Eq. (43). When $\mathcal{N}_x$ is odd, $\Omega_{\mathcal{N}_x}$ is shifted by a constant value, see Eq. (44). This shift (shown by red arrows) is the energy of the domain wall $E_{\rm dw}$.

$$\hat{\Delta} = {\rm diag}(\Delta_1, ..., \Delta_{\mathcal{N}_x}). \tag{41}$$

Constructing the matrix $\hat{H}_{\mathbf{p}\sigma}$ we use periodic boundary conditions in the x direction.

For the system with $\mathcal{N}_x$ unit cells along x axis the grand potential $\Omega_{\mathcal{N}_x}$ (per unit area in y-z plane) is

$$\Omega_{\mathcal{N}_x} = \sum_{\sigma}\sum_{S=1}^{2\mathcal{N}_x}\int \frac{d^2\mathbf{p}}{(2\pi)^2} E^{(S)}_{\mathbf{p}\sigma}\Theta\big(-E^{(S)}_{\mathbf{p}\sigma}\big) + \\ - U\sum_{i_x}\left(\frac{n_{i_x}^2-1}{4} - \frac{\Delta_{i_x}^2}{U^2}\right), \tag{42}$$

where $E^{(S)}_{\mathbf{p}\sigma}$ are the eigenenergies of the matrix $\hat{H}_{\mathbf{p}\sigma}$. To obtain $\Omega_{\mathcal{N}_x}$, the spatial dependencies of the order parameter Δ_{i_x} and the number of electrons per site n_{i_x} minimizing $\Omega_{\mathcal{N}_x}$ are found using a numerical recurrent procedure.

Once $\Omega_{\mathcal{N}_x}$ is known, the energy of a single domain wall $E_{\rm dw}$ can be calculated. To find $E_{\rm dw}$, it is necessary to consider systems with even and odd values of $\mathcal{N}_x$ (this number must be much larger than the width of the domain wall). A system with even $\mathcal{N}_x$ is antiferromagnetically ordered and its grand potential (per unit area in y-z plane) is directly proportional to $\mathcal{N}_x$:

$$\Omega^{\rm even}_{\mathcal{N}_x} = \Omega_0\mathcal{N}_x, \tag{43}$$

where Ω_0 is the grand potential per site of the system with homogeneous SDW ordering. A system with odd number of sites unavoidably contains a domain wall. Therefore

$$\Omega^{\rm odd}_{\mathcal{N}_x} = \Omega_0\mathcal{N}_x + E_{\rm dw}, \tag{44}$$

where $\Omega^{\rm odd}_{\mathcal{N}_x}$ is the grand potential (per unit area in y-z plane) for the systems with odd number of sites and $E_{\rm dw}$ is the energy of the domain wall (per unit area in the wall). The relations (43) and (44) are illustrated in Fig. 3. They allow us to extract $E_{\rm dw}$ from numerical data for $\Omega^{\rm even}$ and $\Omega^{\rm odd}$.

C. Numerical results

Numerically minimizing $\Omega_{\mathcal{N}_x}$, we determine various properties of the studied system. Figure 4 demonstrates the spatial dependence of the order parameter for even and odd $\mathcal{N}_x$. As we can see from Fig. 4(a), the system with even number of sites has the homogeneous SDW order, as in Eq. (7). Naturally, the grand potential for such a state satisfies Eq. (43).

Due to the periodic boundary conditions, a system with odd number of sites cannot maintain unfrustrated antiferromagnetic order, and a domain wall appears. Because of the order parameter frustration, Δ_{i_x} is suppressed inside the domain wall, see Figs. 4(b) and 4(c). In our simulations, we can stabilize both bond-centered and site-centered domain walls. Figure 4(b) illustrates the order parameter structure for the bond-centered domain wall. Such a configuration possesses spatial reflection symmetry with respect to the center of the bond connecting the sites with minimum values of the order parameter. Site-centered domain wall is shown in Fig. 4(c). Spatial inversion relative to central site of the domain wall (the site with vanishing order parameter), accompanied by the spin flip $\mathbf{S} \to -\mathbf{S}$, preserves the site-centered configuration. Since bond-centered and site-centered domain walls have different symmetries, they represent mutually excluding classes of the mean-field solutions. Thus, they must be discussed separately. However, our simulations show that their energies are close to each other.

The domain wall properties are sensitive to the chemical potential. Indeed, Fig. 5 demonstrates the spatial dependencies of the absolute value of the order parameter and the electron density calculated for different values of μ' for the system with $\mathcal{N}_x = 101$, $U/W = 0.17$, and $(t_x, t_y, t_z) = (1.0, 1.0, 0.7)$. One can see from this figure that even small deviation of the chemical potential from zero value sharply changes the order parameter and the electron density inside the domain wall. At higher values of $|\mu'|$ the sensitivity of the order parameter and other quantities becomes less dramatic. Figure 5(a) shows that the order parameter is even function of μ'. Also, this figure demonstrates that the domain wall becomes wider when the chemical potential changes.

The accumulation of the injected charge carriers in the domain wall is illustrated by Fig. 5(b). At half-filling ($\mu' = 0$) there is one electron per site. When the chemical potential changes, the carriers pile up in the domain wall. For positive chemical potentials, the carriers are electrons, and for the negative ones, they are holes. Finally, Fig. 6 presents the domain wall energy and the total charge accumulated inside the domain walls (per unit area in y-z plane) versus the chemical potential in the system with $\mathcal{N}_x = 101$, $U/W = 0.17$, and $(t_x, t_y, t_z) = (1.0, 1.0, 0.7)$.

What can be understood from the numerical data about the properties of a single domain wall? We can see from Fig. 6 that the energy $E_{\rm dw}$ is the even function of the chemical potential. Similarly, Figs. 5(b) and 6(b) show that the accumulated charge is odd function of μ'. These features are consequences of the charge-conjugation symmetry of our model. This symmetry allows us to restrict our attention to positive value of the chemical potential.

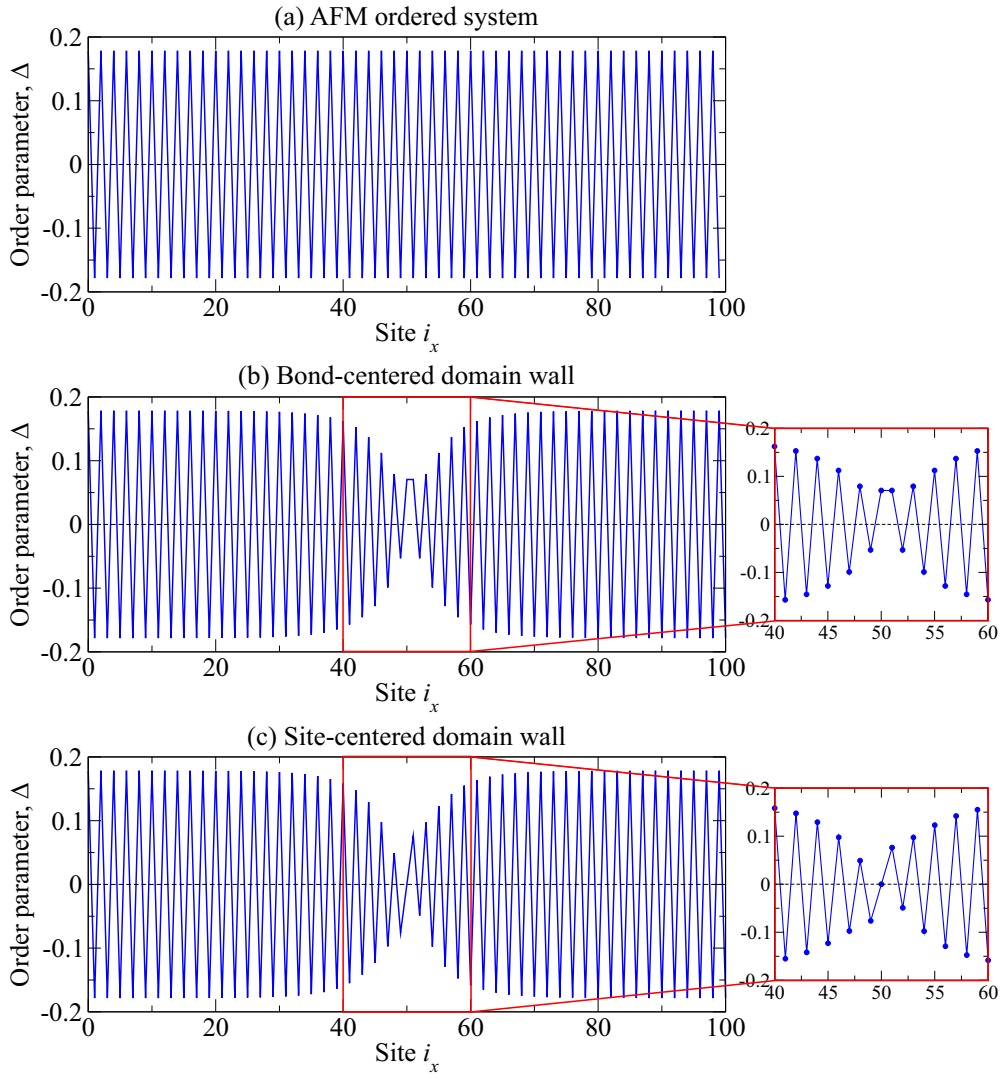

FIG. 4. Spatial variation of the order parameter along x axis, for even and odd values of $\mathcal{N}_x$. (a) When the number of sites in x direction $\mathcal{N}_x$ is even, the antiferromagnetic order parameter maintains the same absolute value for all i_x, while the sign changes from one i_x to the next. The data in the panel is plotted for $\mathcal{N}_x = 100$. [(b), (c)] When $\mathcal{N}_x$ is odd (specifically $\mathcal{N}_x = 101$ for both panels), the antiferromagnetic domain wall emerges. Panel (b) shows the bond-centered domain wall. In the center of such a structure, we see two sites with identical values of the order parameters. The site-centered domain wall is in panel (c). This domain wall is centered on a site with vanishing order parameter. The simulations are performed for $U/W = 0.17$, $(t_x,\ t_y,\ t_z) = (1.0,\ 1.0,\ 0.7)$.

On general grounds, one expects that at zero doping and zero chemical potential, the domain wall energy is positive, meaning that the state with the domain walls is energetically unfavorable. However, as the chemical potential grows, charges dope the domain walls, improving their stability. Figures 6(a) and 6(b) clearly illustrate these tendencies. Most importantly, there is a specific value of μ at which $E_{\rm dw} = 0$. When $E_{\rm dw}$ vanishes, a state with no domain walls and a state with a domain wall are degenerate. The corresponding value of μ is the critical chemical potential $\mu_{\rm dw}$ for the state with domain walls: if $\mu > \mu_{\rm dw}$, the domain wall energy becomes negative, and domain walls carrying finite charge density enter the bulk of the system. As in the previous section,

$$F_{\rm dw} \approx F(0) + \mu_{\rm dw} x, \tag{45}$$

at low x. This equation remains applicable as long as the distance between the domain walls is large, and the interaction between them may be neglected. As the concentration grows, the repulsion between the walls sets in, and Eq. (45) progressively becomes less accurate. In the regime of validity of Eqs. (24), (31), and (45) the competition between the inhomogeneous states is decided by the lowest critical chemical potential, as in Eq. (32).

The critical potential calculated numerically is shown in Fig. 7 for three different anisotropies of "easy-plane" ($t_x = t_y > t_z$) type. We see that the critical chemical potential monotonically increases when the anisotropy increases. To perform consistent comparison of $\mu_{\rm dw}$ with $\mu_{\rm iAF}$ and $\mu_{\rm cAF}$, we need to find $\mu_{\rm dw}$ in the low-U limit, as we did above to obtain the estimates (22) and (30). Numerical calculations at very low U quickly become impossible since the width of the domain wall grows quickly as U drops, and one has to increase the system size stretching computational resources. To circumvent this issue, $\mu_{\rm dw}$ at $U = 0$ is evaluated extrapolating the available

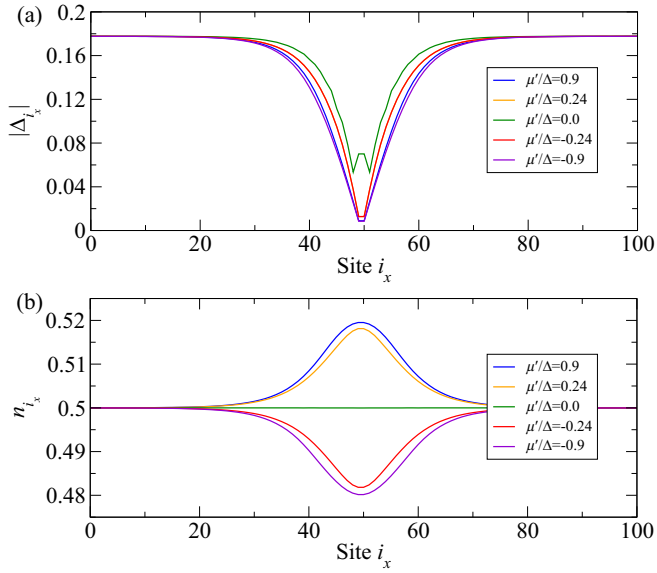

FIG. 5. Spatial dependencies of (a) the absolute values of the order parameter $|\Delta_{i_x}|$, and (b) the electron density n_{i_x}, calculated for the bond-centered domain wall, at different values of the chemical potential μ'. Model parameters are: $U/W = 0.17$, $(t_x,\ t_y,\ t_z) = (1.0,\ 1.0,\ 0.7)$, and $\mathcal{N}_x = 101$.

numerical data to zero value of U. The data points can be adequately fitted by linear functions, see Fig. 7. The resultant low-U values of $\mu_{\rm dw}$ are shown in Fig. 8. Alternatively, the same data can be approximated by a quadratic function. This produces similar values of $\mu_{\rm dw}$, which are also plotted in Fig. 8.

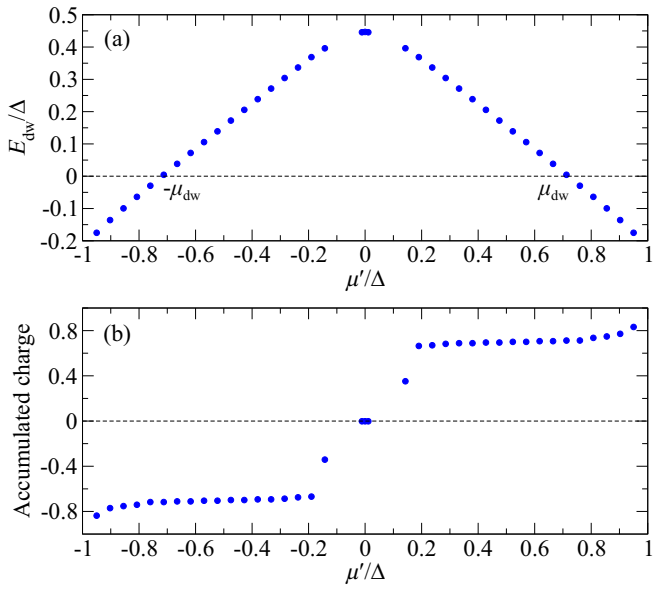

FIG. 6. Chemical potential dependence of (a) the bond-centered domain wall energy $E_{\rm dw}$ and (b) the number of charge carriers in a domain wall. In panel (a) the critical chemical potential $\mu_{\rm dw}$ is marked. It corresponds to the value of μ at which the domain wall energy vanishes. Model parameters are: $\mathcal{N}_x = 101$, $U/W = 0.17$, and $(t_x,\ t_y,\ t_z) = (1.0,\ 1.0,\ 0.7)$.

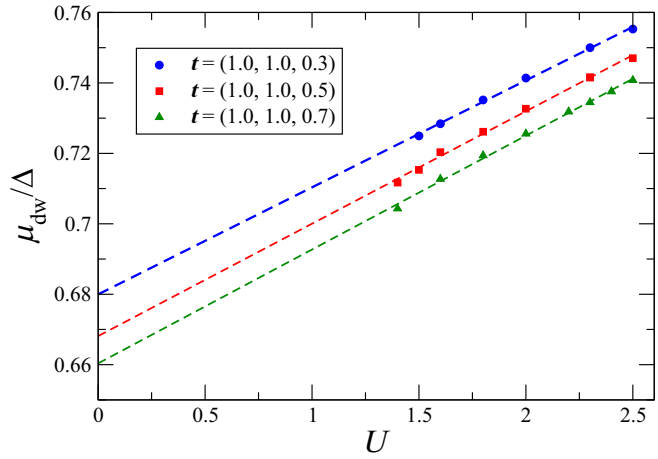

FIG. 7. Critical chemical potential vs interaction constant U for three different anisotropies (see legend). Linear fits are shown as dashed lines.

As long as the anisotropy is not too strong ($t_z > t_x/10$), the critical values of the chemical potential for different phases are ordered according to

$$\mu_{\rm dw} < \mu_{\rm iAF} \lesssim \mu_{\rm cAF}. \tag{46}$$

Thus, for the model under study, the state with the domain wall has the lowest energy, at least at low doping. However, the energy differences separating the most stable phase and metastable "contenders" are insignificant. Indeed,

$$\mu_{\rm iAF} - \mu_{\rm dw} \lesssim 0.06\Delta_0 \tag{47}$$

for all anisotropy parameters. This is presented graphically in Fig. 9. One can see that all critical chemical potentials are tightly packed in a small region between 0 and Δ_0.

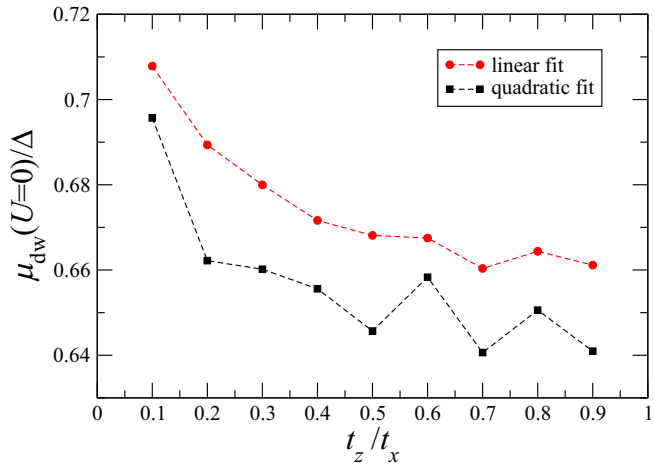

FIG. 8. Critical chemical potential for the state with domain walls $\mu_{\rm dw}$ vs the hopping anisotropy parameter t_z/t_x, in the limit of low U, for the anisotropy of the "easy-plane" ($t_x = t_y > t_z$) type. The data points obtained by linear fit (quadratic function fit) are shown by red circles (black squares).

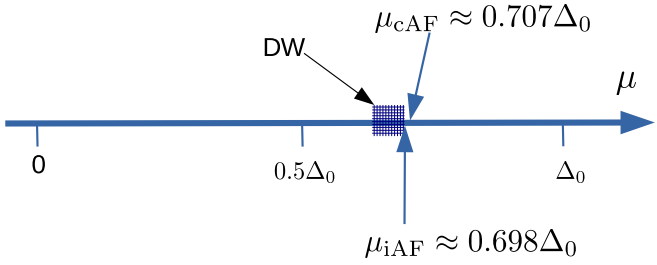

FIG. 9. Locations of the critical chemical potentials for all three inhomogeneous phases. The hatched region represents the interval where $\mu_{\rm dw}$ can be located (depending on the anisotropy). Observe that all critical values are squeezed into a small region of a much larger interval $[0, \Delta_0]$.

V. DISCUSSION AND CONCLUSIONS

In this paper we discuss inhomogeneous phases of the anisotropic Hubbard model in weak-coupling regime. It is known from various studies that a nesting-driven homogeneous SDW, when being doped, loses its stability and yields to an inhomogeneous state. This feature is not unique to the Hubbard Hamiltonian. Other models with nesting demonstrate similar instability. In the context of superconductivity, a related phenomenon exists in the form of inhomogeneous Fulde-Ferrel-Larkin-Ovchinnikov states. Thus, destruction of the electronic liquid homogeneity is not limited to systems modeled by the Hubbard Hamiltonian with repulsion, but rather is of relevance for many situations.

We discuss three specific inhomogeneous phases (two types of phase separated states and the state with domain walls) at zero temperature. It is argued that, at low doping, the free energies of these states can be characterized by a single parameter, critical chemical potential. Such a concept has simple physical meaning: If the chemical potential of a reservoir is lower than the critical chemical potential of a certain inhomogeneous state, doping of our system through formation of this state is impossible. It is clear from this definition that the phase with the lowest critical chemical potential is the most stable at low doping.

The critical chemical potentials for all three phases were evaluated within the mean-field framework. Our calculations demonstrate that the state with domain walls is the most stable. However, since the critical chemical potentials are almost identical [see Eq. (47) and Fig. 9] the energies of the inhomogeneous states are close to each other. The latter property is not limited to the model investigated here: in Ref. [15] the authors cited theoretical evidence available in published literature which suggested that similar "tight competition" between inhomogeneous phases is present in the so-called Rice model [51]. Therefore, we hypothesize that this feature is an intrinsic property of all generic models with nesting and weak coupling.

Since theoretical descriptions of various substances (the Bechgaard salts, iron-based pnictide superconductors) are often use Hamiltonians with nesting, our results have important implications for these materials. Namely, one can argue that purely theoretical prediction of the inhomogeneous phase in a specific material is unreliable, as numerous material factors lie outside the scope of simple theoretical models. We expect that the relative stability of multiple inhomogeneous states, competing to become the true ground state, is affected by the lattice effects, band structure details, Coulomb interaction screening, disorder pinning, and other nonuniversal features.

To illustrate these nonuniversalities, let us briefly examine the role of the long-range Coulomb interaction, which is ignored by the Hubbard-like and other models with purely local interactions. Energy of an inhomogeneous state is unavoidably modified by the long-range Coulomb repulsion. Yet such modification is strongly phase specific. For example, the soliton lattice acquires finite positive contribution to its energy, while any type of phase separation into macroscopic regions of unequal charge density becomes impossible since the corresponding Coulomb energy is extremely large. To reduce this energy, the phase separation instability may reveal itself through formation of mesoscopic structures, like bubbles, columns or slabs, as indeed observed in experiment [23]. These structures compete against the domain wall phase and against each other. This competition occurs within an anisotropic and disordered effective medium created by the host crystal. For a specific material, a reliable prediction of a winner is likely impossible without experimental input.

Our conclusions are not immediately applicable to antiferromagnetic materials *with strong electronic correlations*. The cuprates, whose phenomenology exhibits striking non-mean-field features (e.g., the pseudogap and "the bad metal" state), is one of the most well-known examples of such systems. Beside the cuprates, various iron-based superconducting alloys (particularly, the chalcogenides) are believed to be in the same class. All these compounds are typically modeled by Hubbard-like Hamiltonians with moderate-to-high values of interaction constants. In these regimes the electronic properties are crucially affected by non-mean-field fluctuations that cannot be accounted for within our framework.

However, the discussed theoretical issue remains relevant for these systems as well. Indeed, numerical studies [44,45,49] of the Hubbard Hamiltonian in the strong-coupling regime revealed that several inhomogeneous states with almost identical energies compete against each other to become the true ground state of the Hamiltonian. The diversity of the contending phases can obfuscate the interpretation of experimental data, which may be exemplified by opinion exchange between the authors of Refs. [25,76], and ultimately might indicate the need for alternative approaches in this field of condensed matter physics.

To conclude, we studied inhomogeneous states of the small-U Hubbard model in proximity to the half-filling. We demonstrated that the state with the domain walls is the most stable at low doping. However, the energies of metastable inhomogeneous states are found to be very close to the ground-state energy. We argue that the smallness of this energy separation can introduce significant uncertainty into theoretical modeling of the inhomogeneous states of many-fermions systems with nesting. Numerical evidence of similar energy difference smallness in strong-coupling systems, taken together with our results, seems to suggest that the discussed issue is of broad relevance.

ACKNOWLEDGMENTS

We acknowledge helpful discussions with B.V. Fine. This work is partially supported by the No. 19-52-50015, and RFBR Project RFBR no. 19-02-00421.

APPENDIX A: THE ROLE OF THE FLUCTUATIONS AND THE ACCURACY OF THE MEAN FIELD APPROXIMATION

Theoretical framework outlined in Sec. II, as well as any other version of the mean-field approximation, relies on smallness of fluctuations. Fluctuations-induced corrections to the mean field is an area with long research history, Yet the topic still attracts theorists' attention [77,78]. This attests to a degree of dissatisfaction with the current level of understanding of the importance of non-mean-field (NMF) corrections to the mean-field approximation. Fortunately, despite persistent concerns, various results already available in published literature seem to suggest that NMF physics can be safely incorporated into the mean-field approximation using a simple trick of replacing "bare" model parameters by their "dressed", or effective, counterparts.

This "triviality" of NMF contributions can be illustrated using the findings of Ref. [79], which studied the NMF corrections for the negative-U Hubbard model. The renormalized interaction U' was estimated as

$$|U'| = |U|[1 - 2\ln(2)|U|/W]. \tag{A1}$$

This formula for the effective U' was further employed to evaluate the gap and the transition temperature. Examining Eqs. (43,44,47) of Ref. [79], one can easily recognize the familiar BCS expressions for the order parameter and the transition temperature in which the bare U is replaced by U'. Most revealingly, the ratio $2\Delta/T_c$ was found to be equal to 3.53, as one would expect from an ordinary mean-field scheme, indicating that NMF corrections do not violate the basic structure of the mean-field theory.

Interpreting NMF studies, one should keep in mind that, owing to nonanalytical nature of the mean-field equations, weak modifications to the coupling constant, similar to Eq. (A1), may lead to significant variations of both Δ and T_c. To illustrate this, let us generalize Eq. (A1) as $\lambda' = \lambda + \delta\lambda^{(2)}$, where λ' is the effective dimensionless coupling, $\delta\lambda^{(2)} = c\lambda^2$ is the second-order correction to "bare" λ, and c is a constant independent of λ. We now compare the renormalized gap

$$\Delta \sim We^{-1/(\lambda+\delta\lambda^{(2)})} \tag{A2}$$

(here W is the band width) against the "bare" gap

$$\Delta^{\mathrm{b}} \sim We^{-1/\lambda}. \tag{A3}$$

Since in the weak-coupling regime $1/(\lambda + c\lambda^2) \approx 1/\lambda - c + c^2\lambda$, one derives

$$\Delta \approx \Delta^{\mathrm{b}} \exp(c - c^2\lambda) < \Delta^{\mathrm{b}} \exp(c). \tag{A4}$$

Similar formula for the critical temperature T_c and the corresponding "bare" quantity T_c^{b} reads

$$T_c \approx T_c^{\mathrm{b}} \exp(c - c^2\lambda) < T_c^{\mathrm{b}} \exp(c). \tag{A5}$$

Multiplicative renormalization relations analogous to Eqs. (A4) and (A5) were reported in Refs. [80–84]. Note that, even for moderate values of $|c|$, the renormalizations described by Eqs. (A4) and (A5) may be quite pronounced [curiously, the third-order correction $\delta\lambda^{(3)} = O(\lambda^3)$ always introduces weak modifications to both Δ and T_c, as long as interaction is weak]. For instance, extracting c from expression (A1), one finds $c = -2\ln 2 \approx -1.39$, consequently, $\exp(c) = 0.25$. Thus, in this specific example, the NMF fluctuations depress the gap at least four-fold relative to its "bare" value.

We want to remind the reader here that, despite such a drastic disparity between Δ and Δ^{b}, both these quantities are obtained within identical mean-field framework, the only difference being the use of either renormalized or "bare" coupling constant. In other words, multiplicative renormalizations reported in Refs. [80–84] may look irreconcilable with the mean-field framework, nonetheless, our derivation of Eqs. (A4) and (A5) confirms the mean-field nature of such relations.

Since we study our model at different doping levels, one may ask how the variation of doping change the effective parameters. Fortunately, such changes are unimportant. Indeed, since already (exponentially) weak x is sufficient to induce all phase transitions discussed in this paper, doping-induced corrections are, at best, exponentially weak. As for formal calculations, Ref. [82] established insensitivity of the multiplicative renormalizations to doping. This means that we can treat the effective coupling constant as being independent of doping.

Concluding this analysis of the mean-field renormalization, we would like to mention Ref. [78], which evaluated the effects of Gaussian fluctuations of order parameter. A weak (of order of a percent) correction to the coupling constant was calculated, see Eq. (21) there. Needless to say that in a typical experimentally relevant situation the coupling constant cannot be determined with such an accuracy, limiting the relevance of this correction to purely academic discussions.

The papers cited in this subsection discussed isotropic models. Unlike these, we will investigate the model with quasi-two-dimensional anisotropy. Let us make several remarks in this respect. Even in the extreme limit $t_z = 0$, when the model splits into decoupled planes, Mermin-Wagner theorem does not rule out the ordered state at $T = 0$. However, the fluctuation corrections beyond the mean-field approximation are sensitive to the system's dimensionality (for example, see Eq. (21) of Ref. [78]). Thus, the limit $t_z \to 0$ require special care. On the other hand, at moderate anisotropies $t_z/t \lesssim 1$ we do not expect significant renormalizations coming from the low-dimensional fluctuations. A more detailed study of low-dimensional effects at higher anisotropies is beyond the scope of the present study.

These examples suggest that a mean-field scheme, like the one used in this paper, can easily accommodate the NMF physics: one has to use the renormalized parameters instead of the bare ones. Note that the only place where U' enter our formalism is Eq. (15) for Δ_0, while all other energies are measured in terms of Δ_0. Thus, once NMF contributions are accounted for through Δ_0 renormalizations, all other results presented in this paper require no additional modifications.

APPENDIX B: DETAILS OF THE SOLUTION TO THE GAP EQUATION FOR THE COMMENSURATE SDW STATE

At half-filling ($\mu' = 0$), minimization of the grand potential Ω, Eq. (13), with respect to Δ gives the following equation

$$\frac{\partial\Omega}{\partial\Delta} = \Delta\left[\frac{2}{U} - \int \frac{d^3\mathbf{k}}{(2\pi)^3}\frac{1}{\sqrt{\Delta^2+\varepsilon_{\mathbf{k}}^2}}\right] = 0. \tag{B1}$$

Let us introduce the density of states

$$\rho(\varepsilon) = \int \frac{d^3\mathbf{k}}{(2\pi)^3}\,\delta(\varepsilon - \varepsilon_{\mathbf{k}}). \tag{B2}$$

In the limit of small $\Delta \ll W$ studied here, we can rewrite the integral in the equation (B1) in the form

$$\begin{aligned}
&\int \frac{d^3\mathbf{k}}{(2\pi)^3}\frac{1}{\sqrt{\Delta^2+\varepsilon_{\mathbf{k}}^2}} \\
&= \int_{-W/2}^{W/2} d\varepsilon\,\frac{\rho(\varepsilon)}{\sqrt{\Delta^2+\varepsilon^2}} \\
&\cong \int_{-W/2}^{W/2} d\varepsilon\,\frac{\rho(\varepsilon)-\rho_0}{|\varepsilon|} + \rho_0\int_{-W/2}^{W/2} d\varepsilon\,\frac{1}{\sqrt{\Delta^2+\varepsilon^2}} \\
&\cong \frac{2}{U_c} + 2\rho_0\ln\frac{W}{\Delta},
\end{aligned} \tag{B3}$$

where $\rho_0 = \rho(0)$ is the density of states at the Fermi level, while parameter U_c is defined by the equation

$$\frac{2}{U_c} = \int_{-W/2}^{W/2} d\varepsilon\,\frac{\rho(\varepsilon)-\rho_0}{|\varepsilon|}. \tag{B4}$$

Substituting Eq. (B3) into Eq. (B1), we derive Eq. (15) for the gap at half-filling.

At finite doping, μ' deviates from zero, and the equation for the order parameter can be expressed as

$$2\ln\frac{\Delta_0}{\Delta} = \int_{-W/2}^{W/2} d\varepsilon\,\frac{\Theta(|\mu'|-\sqrt{\Delta^2+\varepsilon^2})}{\sqrt{\Delta^2+\varepsilon^2}}. \tag{B5}$$

Evaluating the integral, one obtains Eq. (14) relating Δ and μ'.

APPENDIX C: DETAILS OF THE MEAN-FIELD FORMALISM FOR THE INCOMMENSURATE SDW STATE

In this Appendix, we will solve Eqs. (29). We start with the observation that in the limit of small $\Delta \ll W$, nesting vector $\mathbf{q}$ is also small: $\mathbf{q} \sim \Delta/W \ll 1$. In this regime, one can write

$$\varepsilon_{\mathbf{k}+\mathbf{q}} \cong \varepsilon_{\mathbf{k}} + \mathbf{q}\frac{\partial\varepsilon_{\mathbf{k}}}{\partial\mathbf{k}}. \tag{C1}$$

Calculating the derivatives of Ω with respect to Δ, $\mathbf{q}$, and μ', and using the smallness of Δ and $\mathbf{q}$ in a manner similar to that described in the Appendix B, we obtain the system of equations:

$$\ln\left(\frac{\Delta_0}{\Delta}\right) = \frac{1}{\rho_0}\int_{-\eta_0}^{\eta_0} d\eta N(0,\eta)\operatorname{arccosh}\left(\frac{|\mu'-q\eta|}{\Delta}\right), \tag{C2}$$

$$q\kappa = \int_{\eta_0}^{\eta_0} d\eta N(0,\eta)\eta\sqrt{(\mu'-q\eta)^2-\Delta^2}\operatorname{sign}(q\eta-\mu'), \tag{C3}$$

$$x = 2\int_{\eta_0}^{\eta_0} d\eta N(0,\eta)\sqrt{(\mu'-q\eta)^2-\Delta^2}\operatorname{sign}(\mu'-q\eta), \tag{C4}$$

where we introduce the joint density of states

$$N(\xi,\eta) = \int \frac{d^3\mathbf{k}}{(2\pi)^3}\,\delta(\xi-\varepsilon_{\mathbf{k}})\delta\left[\eta + \hat{n}_{\mathbf{q}}\frac{\partial\varepsilon_{\mathbf{k}}}{\partial\mathbf{k}}\right], \tag{C5}$$

$$\eta_0 = \max_{\mathbf{k}}\left(\hat{n}_{\mathbf{q}}\frac{\partial\varepsilon_{\mathbf{k}}}{\partial\mathbf{k}}\right), \quad \kappa = \int_{-\eta_0}^{\eta_0} d\eta N(0,\eta)\eta^2, \tag{C6}$$

and the unit vector $\hat{n}_{\mathbf{q}} = \mathbf{q}/|\mathbf{q}|$ is collinear with $\mathbf{q}$.

Equations (C2), (C3), and (C4) form a closed system of equations for self-consistent determination of $\Delta(x)$, $\mu(x)$, and $q(x) = |\mathbf{q}(x)|$ at the fixed direction of the nesting vector $\mathbf{q}$. We solve this system of equations for $(t_x, t_y, t_z) = (1, 1, 0.7)$, and for two directions of $\mathbf{q}$: parallel to the z axis and parallel to the y axis. At relatively large doping, the state with $\mathbf{q}$ parallel to the z axis is energetically more favorable, while at small doping the situation is opposite. However, the difference in free energies between these two cases turn out to be negligibly small. For the z axis orientation, the data is shown in Fig. 2.

[1] X. Zheng, C. Xu, Y. Tomokiyo, E. Tanaka, H. Yamada, and Y. Soejima, Observation of Charge Stripes in Cupric Oxide, Phys. Rev. Lett. **85**, 5170 (2000).

[2] J. Tranquada, B. Sternlieb, J. Axe, Y. Nakamura, and S. Uchida, Evidence for stripe correlations of spins and holes in copper oxide superconductors, Nature (London) **375**, 561 (1995).

[3] A. Bianconi, N. Saini, A. Lanzara, M. Missori, T. Rossetti, H. Oyanagi, H. Yamaguchi, K. Oka, and T. Ito, Determination of the Local Lattice Distortions in the CuO_2 Plane of $La_{1.85}Sr_{0.15}CuO_4$, Phys. Rev. Lett. **76**, 3412 (1996).

[4] A. Li, J.-X. Yin, J. Wang, Z. Wu, J. Ma, A. S. Sefat, B. C. Sales, D. G. Mandrus, M. A. McGuire, R. Jin, C. Zhang, P. Dai, B. Lv, C.-W. Chu, X. Liang, P.-H. Hor, C.-S. Ting, and S. H. Pan, Surface terminations and layer-resolved tunneling spectroscopy of the 122 iron pnictide superconductors, Phys. Rev. B **99**, 134520 (2019).

[5] J. Dho, Y. Kim, Y. Hwang, J. Kim, and N. Hur, Strain-induced magnetic stripe domains in $La_{0.7}Sr_{0.3}MnO_3$ thin films, Appl. Phys. Lett. **82**, 1434 (2003).

[6] T. Miao, L. Deng, W. Yang, J. Ni, C. Zheng, J. Etheridge, S. Wang, H. Liu, H. Lin, Y. Yu *et al.*, Direct experimental evidence of physical origin of electronic phase separation in manganites, Proc. Natl. Acad. Sci. U.S.A. **117**, 7090 (2020).

[7] Y. Zhu, K. Du, J. Niu, L. Lin, W. Wei, H. Liu, H. Lin, K. Zhang, T. Yang, Y. Kou *et al.*, Chemical ordering suppresses

large-scale electronic phase separation in doped manganites, Nat. Commun. **7**, 11260 (2016).

[8] K. Iwaya, R. Shimizu, T. Ohsawa, T. Hashizume, and T. Hitosugi, Stripe charge ordering in SrO-terminated $SrTiO_3$ (001) surfaces, Phys. Rev. B **83**, 125117 (2011).

[9] M. Sing, H. O. Jeschke, F. Lechermann, R. Valentí, and R. Claessen, Influence of oxygen vacancies on two-dimensional electron systems at $SrTiO_3$-based interfaces and surfaces, Eur. Phys. J.: Spec. Top. **226**, 2457 (2017).

[10] Y. Laplace, J. Bobroff, V. Brouet, G. Collin, F. Rullier-Albenque, D. Colson, and A. Forget, Nanoscale-textured superconductivity in Ru-substituted $BaFe_2As_2$: A challenge to a universal phase diagram for the pnictides, Phys. Rev. B **86**, 020510(R) (2012).

[11] S. Kokanova and A. Rozhkov, Disorder correction to the Néel temperature of ruthenium-doped $BaFe_2As_2$: Theoretical analysis, Phys. Rev. B **99**, 075134 (2019).

[12] Q. Luo and E. Dagotto, Magnetic phase diagram of a five-orbital Hubbard model in the real-space Hartree-Fock approximation varying the electronic density, Phys. Rev. B **89**, 045115 (2014).

[13] A. Bianconi, N. Poccia, A. O. Sboychakov, A. L. Rakhmanov, and K. I. Kugel, Intrinsic arrested nanoscale phase separation near a topological Lifshitz transition in strongly correlated two-band metals, Supercond. Sci. Technol. **28**, 024005 (2015).

[14] A. Sboychakov, Phase separation in strongly correlated electron systems with wide and narrow bands: A comparison of the Hubbard-I and DMFT approximations, Physica B **417**, 49 (2013).

[15] A. L. Rakhmanov, A. V. Rozhkov, A. O. Sboychakov, and F. Nori, Phase separation of antiferromagnetic ground states in systems with imperfect nesting, Phys. Rev. B **87**, 075128 (2013).

[16] P. A. Igoshev, M. A. Timirgazin, V. F. Gilmutdinov, A. K. Arzhnikov, and V. Y. Irkhin, Spiral magnetism in the single-band Hubbard model: The Hartree-Fock and slave-boson approaches, J. Phys.: Condens. Matter **27**, 446002 (2015).

[17] D. E. Sheehy and L. Radzihovsky, BEC-BCS crossover, phase transitions and phase separation in polarized resonantly-paired superfluids, Ann. Phys. **322**, 1790 (2007).

[18] A. Kornilov, V. Pudalov, Y. Kitaoka, K. Ishida, G.-q. Zheng, T. Mito, and J. S. Qualls, Coexistence of antiferromagnetic and paramagnetic electronic phases in quasi-one-dimensional $(TMTSF)_2PF_6$, JETP Lett. **78**, 21 (2003).

[19] N. Kang, B. Salameh, P. Auban-Senzier, D. Jérome, C. Pasquier, and S. Brazovskii, Domain walls at the spin-density-wave endpoint of the organic superconductor $(TMTSF)_2PF_6$ under pressure, Phys. Rev. B **81**, 100509(R) (2010).

[20] B. Salameh, P. Auban-Senzier, N. Kang, C. Pasquier, and D. Jérome, Precise texture determination of the spin density wave/superconductivity mixture in the phase separation regime of $(TMTSF)_2PF_6$, Phys. B: Condens. Matter **404**, 476 (2009).

[21] A. V. Kornilov, V. M. Pudalov, Y. Kitaoka, K. Ishida, G.-q. Zheng, T. Mito, and J. S. Qualls, Macroscopically inhomogeneous state at the boundary between the superconducting, antiferromagnetic, and metallic phases in quasi-one-dimensional $(TMTSF)_2PF_6$, Phys. Rev. B **69**, 224404 (2004).

[22] Y. A. Gerasimenko, S. V. Sanduleanu, V. A. Prudkoglyad, A. V. Kornilov, J. Yamada, J. S. Qualls, and V. M. Pudalov, Coexistence of superconductivity and spin-density wave in $(TMTSF)_2ClO_4$: Spatial structure of the two-phase state, Phys. Rev. B **89**, 054518 (2014).

[23] A. Narayanan, A. Kiswandhi, D. Graf, J. Brooks, and P. Chaikin, Coexistence of Spin Density Waves and Superconductivity in $(TMTSF)_2PF_6$, Phys. Rev. Lett. **112**, 146402 (2014).

[24] S. A. Kivelson, I. P. Bindloss, E. Fradkin, V. Oganesyan, J. Tranquada, A. Kapitulnik, and C. Howald, How to detect fluctuating stripes in the high-temperature superconductors, Rev. Mod. Phys. **75**, 1201 (2003).

[25] R. Comin, R. Sutarto, E. H. da Silva Neto, L. Chauviere, R. Liang, W. N. Hardy, D. A. Bonn, F. He, G. A. Sawatzky, and A. Damascelli, Broken translational and rotational symmetry via charge stripe order in underdoped $YBa_2Cu_3O_{6+y}$, Science **347**, 1335 (2015).

[26] B. V. Fine, Magnetic vortices instead of stripes: Another interpretation of magnetic neutron scattering in lanthanum cuprates, Phys. Rev. B **75**, 060504(R) (2007).

[27] H. Schulz, Domain walls in a doped antiferromagnet, J. Phys. France **50**, 2833 (1989).

[28] J. Zaanen and O. Gunnarsson, Charged magnetic domain lines and the magnetism of high-T_c oxides, Phys. Rev. B **40**, 7391 (1989).

[29] G. Allodi, R. De Renzi, G. Guidi, F. Licci, and M. W. Pieper, Electronic phase separation in lanthanum manganites: Evidence from ^{55}Mn NMR, Phys. Rev. B **56**, 6036 (1997).

[30] E. Dagotto, *Nanoscale Phase Separation and Colossal Magnetoresistance: The Physics of Manganites and Related Compounds*, Vol. 136 (Springer Science & Business Media, New York, 2013).

[31] M. Hennion, F. Moussa, G. Biotteau, J. Rodríguez-Carvajal, L. Pinsard, and A. Revcolevschi, Evidence of anisotropic magnetic polarons in $La_{0.94}Sr_{0.06}MnO_3$ by neutron scattering and comparison with Ca-doped manganites, Phys. Rev. B **61**, 9513 (2000).

[32] K. I. Kugel, A. L. Rakhmanov, and A. O. Sboychakov, Phase Separation in Jahn-Teller Systems with Localized and Itinerant Electrons, Phys. Rev. Lett. **95**, 267210 (2005).

[33] A. O. Sboychakov, K. I. Kugel, and A. L. Rakhmanov, Jahn-Teller distortions and phase separation in doped manganites, Phys. Rev. B **74**, 014401 (2006).

[34] J. T. Park, D. S. Inosov, C. Niedermayer, G. L. Sun, D. Haug, N. B. Christensen, R. Dinnebier, A. V. Boris, A. J. Drew, L. Schulz, T. Shapoval, U. Wolff, V. Neu, X. Yang, C. T. Lin, B. Keimer, and V. Hinkov, Electronic Phase Separation in the Slightly Underdoped Iron Pnictide Superconductor $Ba_{1-x}K_xFe_2As_2$, Phys. Rev. Lett. **102**, 117006 (2009).

[35] A. O. Sboychakov, A. V. Rozhkov, K. I. Kugel, A. L. Rakhmanov, and F. Nori, Electronic phase separation in iron pnictides, Phys. Rev. B **88**, 195142 (2013).

[36] L. P. Gor'kov and G. B. Teitel'baum, Spatial inhomogeneities in iron pnictide superconductors: The formation of charge stripes, Phys. Rev. B **82**, 020510(R) (2010).

[37] A. Gorbatsevich, Y. Kopaev, and I. Tokatly, Band theory of phase stratification, Zh. Eksp. Teor. Fiz. **101**, 971 (1992) [Sov. Phys. JETP **74**, 521 (1992)].

[38] P. A. Igoshev, M. A. Timirgazin, A. A. Katanin, A. K. Arzhnikov, and V. Y. Irkhin, Incommensurate magnetic order and phase separation in the two-dimensional Hubbard model with nearest- and next-nearest-neighbor hopping, Phys. Rev. B **81**, 094407 (2010).

[39] P. E. Dolgirev and B. V. Fine, Pseudogap and Fermi surface in the presence of a spin-vortex checkerboard for 1/8-doped lanthanum cuprates, Phys. Rev. B **96**, 075137 (2017).

[40] A. V. Aristova, V. K. Bhartiya, and B. V. Fine, Modeling superconductivity in the background of a spin-vortex checkerboard, Phys. Rev. B **100**, 174503 (2019).

[41] B. V. Fine, Implications of spin vortex scenario for 1/8-doped lanthanum cuprates, J. Supercond. Novel Magn. **24**, 1207 (2011).

[42] A. L. Rakhmanov, K. I. Kugel, and A. O. Sboychakov, Coexistence of spin density wave and metallic phases under pressure, J. Supercond. Novel Magn. **33**, 2405 (2020).

[43] A. Buzdin and V. Tugushev, Phase diagrams of electronic and superconducting transitions to soliton lattice states, Sov. Phys. JETP **58**, 428 (1983).

[44] H.-H. Zhao, K. Ido, S. Morita, and M. Imada, Variational Monte Carlo method for fermionic models combined with tensor networks and applications to the hole-doped two-dimensional Hubbard model, Phys. Rev. B **96**, 085103 (2017).

[45] B.-X. Zheng, C.-M. Chung, P. Corboz, G. Ehlers, M.-P. Qin, R. M. Noack, H. Shi, S. R. White, S. Zhang, and G. K.-L. Chan, Stripe order in the underdoped region of the two-dimensional Hubbard model, Science **358**, 1155 (2017).

[46] A. Himeda, T. Kato, and M. Ogata, Stripe States with Spatially Oscillating d-Wave Superconductivity in the Two-Dimensional $t-t'-J$ Model, Phys. Rev. Lett. **88**, 117001 (2002).

[47] P. Corboz, T. M. Rice, and M. Troyer, Competing States in the t-J Model: Uniform d-Wave State versus Stripe State, Phys. Rev. Lett. **113**, 046402 (2014).

[48] C.-P. Chou, N. Fukushima, and T. K. Lee, Cluster-glass wave function in the two-dimensional extended t-J model, Phys. Rev. B **78**, 134530 (2008).

[49] J. P. F. LeBlanc, A. E. Antipov, F. Becca, I. W. Bulik, G. K.-L. Chan, C. M. Chung, Y. Deng, M. Ferrero, T. M. Henderson, C. A. Jimenez-Hoyos, E. Kozik, X. W. Liu, A. J. Millis, N. V. Prokofev, M. Qin, G. E. Scuseria, H. Shi, B. V. Svistunov, L. F. Tocchio, I. S. Tupitsyn, S. R. White, S. Zhang, B. X. Zheng, Z. Zhu, and E. Gull (Simons Collaboration on the Many-Electron Problem), Solutions of the Two-Dimensional Hubbard Model: Benchmarks and Results from a Wide Range of Numerical Algorithms, Phys. Rev. X **5**, 041041 (2015).

[50] E. Dagotto, Complexity in strongly correlated electronic systems, Science **309**, 257 (2005).

[51] T. M. Rice, Band-structure effects in itinerant antiferromagnetism, Phys. Rev. B **2**, 3619 (1970).

[52] A. V. Rozhkov, A. L. Rakhmanov, A. O. Sboychakov, K. I. Kugel, and F. Nori, Spin-Valley Half-Metal as a Prospective Material for Spin Valleytronics, Phys. Rev. Lett. **119**, 107601 (2017).

[53] Y.-D. Chuang, A. D. Gromko, D. S. Dessau, T. Kimura, and Y. Tokura, Fermi surface nesting and nanoscale fluctuating charge/orbital ordering in colossal magnetoresistive oxides, Science **292**, 1509 (2001).

[54] M. L. Kiesel, C. Platt, W. Hanke, D. A. Abanin, and R. Thomale, Competing many-body instabilities and unconventional superconductivity in graphene, Phys. Rev. B **86**, 020507(R) (2012).

[55] F. Šimkovic IV, X.-W. Liu, Y. Deng, and E. Kozik, Ground-state phase diagram of the repulsive fermionic $t-t'$ Hubbard model on the square lattice from weak coupling, Phys. Rev. B **94**, 085106 (2016).

[56] K. S. Mosoyan, A. V. Rozhkov, A. O. Sboychakov, and A. L. Rakhmanov, Spin-density wave state in simple hexagonal graphite, Phys. Rev. B **97**, 075131 (2018).

[57] A. L. Rakhmanov, A. O. Sboychakov, K. I. Kugel, A. V. Rozhkov, and F. Nori, Spin-valley half-metal in systems with Fermi surface nesting, Phys. Rev. B **98**, 155141 (2018).

[58] R. Nandkishore, G.-W. Chern, and A. V. Chubukov, Itinerant Half-Metal Spin-Density-Wave State on the Hexagonal Lattice, Phys. Rev. Lett. **108**, 227204 (2012).

[59] A. O. Sboychakov, A. L. Rakhmanov, K. I. Kugel, A. V. Rozhkov, and F. Nori, Magnetic field effects in electron systems with imperfect nesting, Phys. Rev. B **95**, 014203 (2017).

[60] J. González and T. Stauber, Kohn-Luttinger Superconductivity in Twisted Bilayer Graphene, Phys. Rev. Lett. **122**, 026801 (2019).

[61] A. O. Sboychakov, A. V. Rozhkov, A. L. Rakhmanov, and F. Nori, Externally Controlled Magnetism and Band Gap in Twisted Bilayer Graphene, Phys. Rev. Lett. **120**, 266402 (2018).

[62] A. L. Rakhmanov, K. I. Kugel, M. Y. Kagan, A. V. Rozhkov, and A. O. Sboychakov, Inhomogeneous electron states in the systems with imperfect nesting, JETP Lett. **105**, 806 (2017).

[63] R. S. Akzyanov, A. O. Sboychakov, A. V. Rozhkov, A. L. Rakhmanov, and F. Nori, AA-stacked bilayer graphene in an applied electric field: Tunable antiferromagnetism and coexisting exciton order parameter, Phys. Rev. B **90**, 155415 (2014).

[64] A. O. Sboychakov, A. L. Rakhmanov, A. V. Rozhkov, and F. Nori, Metal-insulator transition and phase separation in doped AA-stacked graphene bilayer, Phys. Rev. B **87**, 121401(R) (2013).

[65] A. V. Rozhkov, Superconductivity without attraction in a quasi-one-dimensional metal, Phys. Rev. B **79**, 224520 (2009).

[66] A. V. Rozhkov, Competition between different order parameters in a quasi-one-dimensional superconductor, Phys. Rev. B **79**, 224501 (2009).

[67] A. V. Rozhkov, Variational description of the dimensional crossover in an array of coupled one-dimensional conductors, Phys. Rev. B **68**, 115108 (2003).

[68] P. Hirschfeld, M. Korshunov, and I. Mazin, Gap symmetry and structure of Fe-based superconductors, Rep. Prog. Phys. **74**, 124508 (2011).

[69] R. M. Fernandes and J. Schmalian, Competing order and nature of the pairing state in the iron pnictides, Phys. Rev. B **82**, 014521 (2010).

[70] G. Grüner, *Density Waves In Solids* (Addison-Wesley Publishing Company, Reading, MA, 1994).

[71] D. A. Khokhlov, A. L. Rakhmanov, A. V. Rozhkov, and A. O. Sboychakov, Dynamical spin susceptibility of spin-valley half-metal, Phys. Rev. B **101**, 235141 (2020).

[72] A. O. Sboychakov, A. V. Rozhkov, A. L. Rakhmanov, and F. Nori, Antiferromagnetic states and phase separation in doped AA-stacked graphene bilayers, Phys. Rev. B **88**, 045409 (2013).

[73] S. A. Brazovskii, L. P. Gor'kov, and J. R. Schrieffer, Influence of interchain electron hopping on commensurate one-dimensional conductors, Phys. Scr. **25**, 423 (1982).

[74] D. Baeriswyl, D. K. Campbell, J. M. Carmelo, F. Guinea, and E. Louis, *The Hubbard Model: Its Physics and Mathematical Physics*, Vol. 343 (Springer Science & Business Media, New York, 2013).

[75] M. Kato, K. Machida, H. Nakanishi, and M. Fujita, Soliton lattice modulation of incommensurate spin density wave in two dimensional Hubbard model-a mean field study, J. Phys. Soc. Jpn. **59**, 1047 (1990).

[76] B. V. Fine, Comment on 'Broken translational and rotational symmetry via charge stripe order in underdoped $YBa_2Cu_3O_{6+y}$', Science **351**, 235 (2016).

[77] S. Fischer, M. Hecker, M. Hoyer, and J. Schmalian, Short-distance breakdown of the Higgs mechanism and the robustness of the BCS theory for charged superconductors, Phys. Rev. B **97**, 054510 (2018).

[78] M. Hoyer and J. Schmalian, Role of fluctuations for density-wave instabilities: Failure of the mean-field description, Phys. Rev. B **97**, 224423 (2018).

[79] A. Martín-Rodero and F. Flores, Solution for the U-negative Hubbard superconductor including second-order correlation effects, Phys. Rev. B **45**, 13008 (1992).

[80] P. G. J. van Dongen, Thermodynamics of the Extended Hubbard Model in High Dimensions, Phys. Rev. Lett. **67**, 757 (1991).

[81] P. G. J. van Dongen, Extended Hubbard model at weak coupling, Phys. Rev. B **50**, 14016 (1994).

[82] P. G. J. van Dongen, Phase Separation in the Extended Hubbard Model at Weak Coupling, Phys. Rev. Lett. **74**, 182 (1995).

[83] T. Schauerte and P. G. J. van Dongen, Symmetry breaking in the Hubbard model at weak coupling, Phys. Rev. B **65**, 081105(R) (2002).

[84] J. K. Freericks and M. Jarrell, Magnetic Phase Diagram of the Hubbard Model, Phys. Rev. Lett. **74**, 186 (1995).